ISSN 1069-3513, Izvestiya, Physics of the Solid Earth, 2016, Vol. 52, No. 4, pp. 572–589. © Pleiades Publishing, Ltd., 2016.
Original Russian Text © T.S. Sakoulina, S.N. Kashubin, G.A. Pavlenkova, 2016, published in Fizika Zemli, 2016, No. 4, pp. 107–124.

Deep Seismic Soundings on the 1-AP Profile in the Barents Sea: Methods and Results

T. S. Sakoulina[a], S. N. Kashubin[b], and G. A. Pavlenkova[c]

[a] *Sevmorgeo Rosnedra, ul. Rozenshteina 36, St. Petersburg, 198095 Russia*
e-mail: Sakoulina@sevmorgeo.com

[b] *Karpinsky Russian Geological Research Institute (VSEGEI), Srednii prosp. 76, St. Petersburg, 199106 Russia*
e-mail: Sergei_Kashubin@vsegei.com

[c] *Schmidt Institute of Physics of the Earth, Russian Academy of Sciences, ul. B. Gruzinskaya 10, Moscow, 123995 Russia*
e-mail: gpavlenkova@yandex.ru

Received June 1, 2015

Abstract—Profile 1-AP with a length of 1300 km intersects the Barents Sea from The Kola Peninsula to Franz Josef Land. The combined Common Depth Point (CDP) and Deep Seismic Sounding (DSS) seismic studies were carried out on this profile. The DSS measurements were conducted with the standalone bottom seismic stations with an interval of 5–20 km between them. The stations recorded the signals generated by the large air guns with a step of 250 m. Based on these data, the detailed *P*-velocity section of the Earth's crust and uppermost mantle have been constructed for the entire profile and the *S*-velocity section for its southern part. The use of a variety of methods for constructing the velocity sections enabled us to assess the capabilities of each method from the standpoint of the highest reliability and informativity of the models. The ray tracing method yielded the best results. The 1-PR profile crosses two large basins—the South Barents and North Barents ones, with the thickness of the sediments increasing from 8 to 10 km in the south to 12–15 km in the north. The Earth's crust pertains to the continental type along the entire profile. Its thickness averages 32 to 36 km and only increases to 43 km at the boundary between the two basins. The distinct change in the wave field at this boundary suggests the presence of a large deep fault in this zone. The high-velocity blocks are revealed in the crust of the South Barents basin, whereas the North Barents crust is characterized by relatively low velocities.

Keywords: Earth's crust, deep seismic sounding, velocity modeling, deep basins, Barents Sea

DOI: 10.1134/S106935131604008X

INTRODUCTION

The combined deep seismic studies by the common depth point (CDP) and deep seismic sounding (DSS) methods along the 1-AP profile in the Barents Sea have been carried out by Sevmorgeo enterprise (St. Petersburg) in 1995–2002 (Fig. 1). The works were conducted in collaboration with the Institute of Oceanology (IO) of the Russian Academy of Sciences (RAS) (Moscow), Nevskgeologiya (St. Peterburg), Tekhmorgeo (Murmansk), Rudgeofizika (St.-Petersburg), and Sevmorneftegeofizika enterprises (Murmansk).

These works were the first marine combined CDP-DSS surveys carried out under the state program on developing a network of reference profiles and superdeep parametric wells. The DSS studies on the 1-AP profile addressed the experimental and methodological issues. The seismic signals in these studies were generated by large air guns and recorded by different types of bottom seismic stations, which were mainly designed by the participating organizations. The detailed measurement schemes were applied (Sakoulina et al., 1999; 2000; 2003). Subsequently, the 1-AP profile was complemented by another three reference profiles in the Barents-Kara Sea region (Ivanova et al., 2006; Sakoulina et al., 2009; Roslov et al., 2009). Earlier, the DSS studies with the explosion sources and bottom recording stations were carried out in this region by the Schmidt Institute of Physics of the Earth (IPE) RAS and IO RAS. The 600-km DSS-76 profile coinciding with the southern segment of the 1-AP geotraverse was shot in 1976 (Davidova et al., 1985; Davidova and Mikhota, 1986). In 1982, the measurements were carried out on the DSS-82 profile with a length of 800 km, which crosses the South Barents Basin (Morozova et al., 1995).

The 1-AP profile extends for a total length of 1440 km, including 1330 km in the sea and 110 km inland. At the southern end, the profile intercepts the SG-3 cross section of the Kola Superdeep Borehole (at the town of Zapolyarnyi). In the north, it abuts on the cross section of the Hayes-1 parametric well on Franz Josef

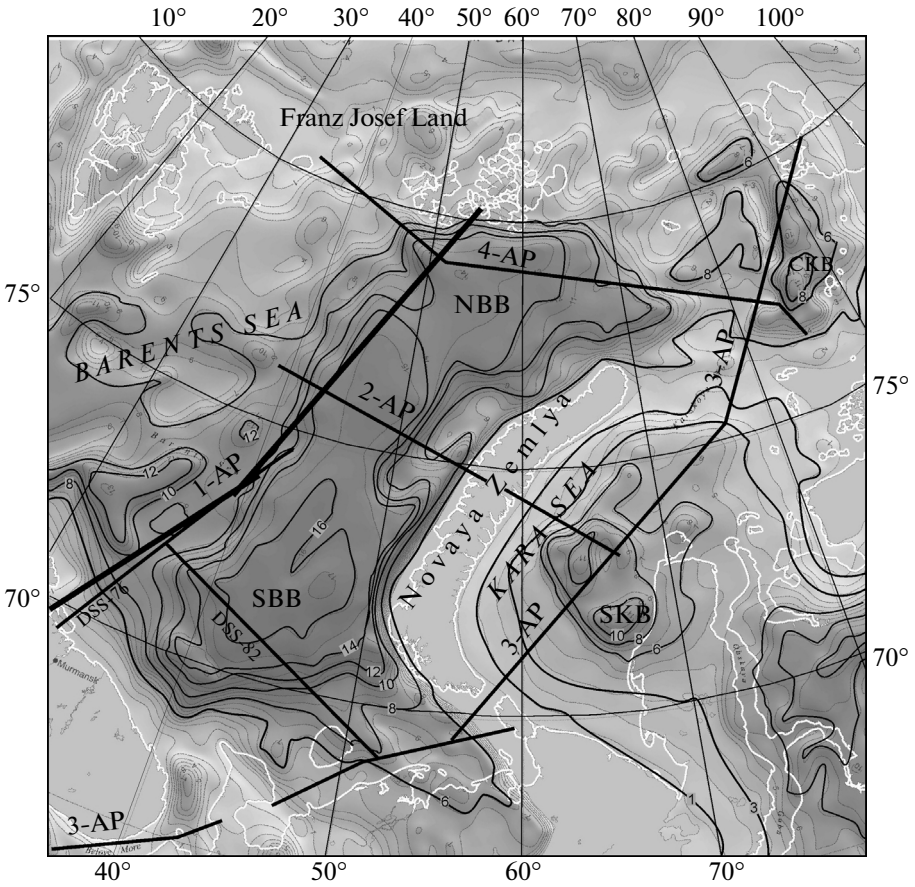

Fig. 1. The layout of the profiles of deep seismic soundings in the Barents–Kara region and the map of the thickness of the sedimentary cover (in km). 1-AP, 2-AP, 3-AP, and 4-AP are the CDP and DSS profiles surveyed by Sevmorgeo; DSS-76 and DSS-82 are the profiles studied by IPE RAS and IO RAS in 1976 and 1982. Basins: SBB, the South Barents Basin; NBB, the North Barents Basin; SKB, the South Kara Basin; NKB, the North Kara Basin. Profile 1-AP s indicated by the heavy line.

Land. The profile passes through the northern margin of the Baltic shield (the Kola-Kanin monocline) and the deep basins of the Barents Sea: the northwestern limb of the South Barents Basin and the North Barents Basin (Fig. 1). The thickness of the sediments increases along the profile from 0 to 12–15 km and, according to the detailed CDP–DSS studies, the structure of the basement and sedimentary cover sharply varies within these basins along the profile (Fig. 2).

The DSS studies within the offshore part of the 1-AP line were aimed at exploring the structure of the crust and uppermost mantle in the Barents Sea basins and uncovering the probable history of their formation.

The seismic signal was generated by the large air gun sources with a gun volume of 80 to 120 liters, which ensured the necessary depth of the survey. The air-gun shots were produced at a time interval of 2 min, which corresponds to 250 m in the plane. The seismic signal was detected and recorded by the various designs of standalone bottom seismic stations (SBSS), which mainly differed by the type of recording (digital or analog) and the number of the recorded components from the minimal single-component (vertical component Z of the displacement vector) to the maximal four-component (three components of the displacement vector X, Y, and Z, as well as the confining pressure component H). The spacing between the stations was 5 km in the southern offshore part of the profile (shot points (SPs) 0 to 150 km) for illuminating the land–sea transition zone and mainly 20 km in the remaining part.

Hence, a very dense (for the deep seismic surveys) measurement configuration was implemented on the 1-AP profile. In the seismograms corresponding to a common receiving point (in the case of the inverted system), seismic records were obtained with a step of 250 m and wave tracking at the large source–receiver distances: the length of the travel-time curves was mainly within 100–150 km, maximally up to 200–250 km. The typical stacks of the seismograms obtained on the different segments of the profile are shown in Fig. 3.

The first full analysis of the 1-AP DSS data, from seismic record preprocessing to reconstructing the crustal cross sections by the different kinematic inversion methods was carried out in Sevmorgeo. The

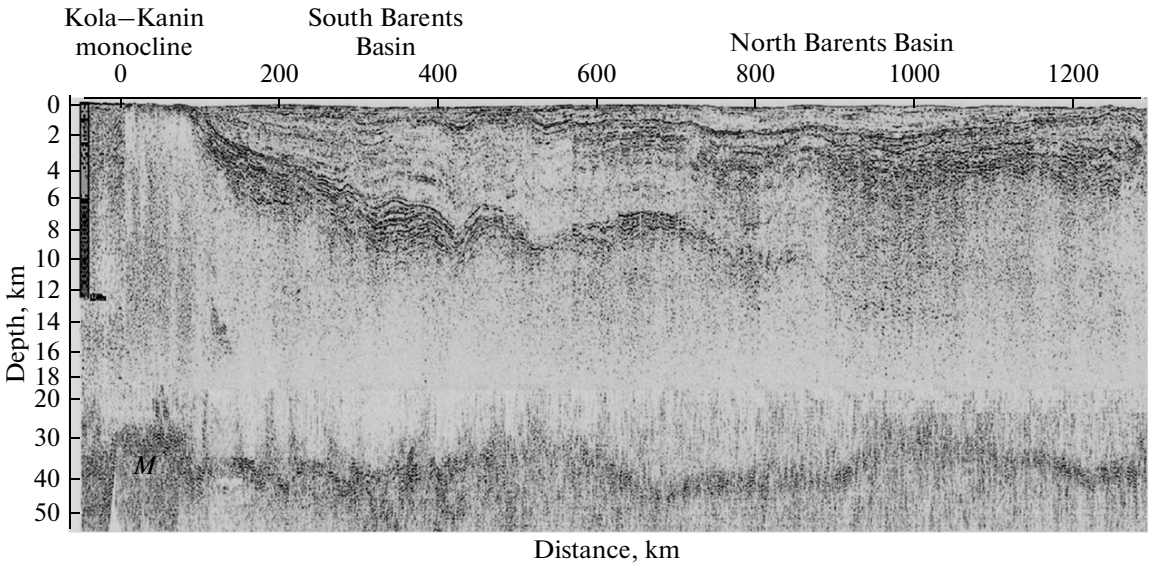

Fig. 2. The crustal wave section along the 1-AP profile constructed from the pre-critical reflections (CDP) data for the depth interval 0–16 km and from the post-critical reflected waves from the bottom portions of the crust and M-boundary in the depth interval from 16 to 50 km (DSS data).

results were partially published (Verba et al., 2001; Sakoulina et al., 2003; Matveev et al., 2005; Ivanova et al., 2006). Subsequently, the DSS data were reinterpreted. The reinterpretation included construction of the velocity section based on the ray tracing the solution of the direct problem for the *P*-waves (Sevmorgeo, IPE RAS). The solution in the southern part of the profile was obtained for the shear (converted) waves (VSEGEI).

In the present work, we discuss the results of all the studies carried out on the 1-AP DSS profile, including the CDP reflection data. The velocity sections for the southern part of the 1-AP line are compared to the results of the processing along the DSS-76 profile.

Particular attention is focused on the methodical questions, assessing the informativity and reliability of DSS data processing and interpretation, exploring the possibilities of using the *S*-wave field in the marine surveys, and revealing the most challenging problems in the identification of the origin of the recorded waves and the general variability of the wave fields. In conclusion, the geological and geophysical results of the studies on the 1-AP line are discussed.

THE OUTLINE OF THE *P*-WAVE SEISMIC DATA

The obtained DSS records contain all the main compression (*P*-) waves which characterize the key structural features of the Earth's crust (Fig. 3). The first arrivals present the reflected waves in the sediments *P*sed, in the crystalline crust *P*g, and in the uppermost mantle (*P*n); the second arrivals show the waves reflected from the crustal bottom, from the Moho (*P*mP), from the intermediate crustal interfaces K1 and K2, etc.

The kinematic characteristics of all these wave types significantly vary along the profile. This primarily concerns the *P*g phase and is due to the changes in the basement structure. The regular changes appearing in the shape of the travel-time curves mark the crustal blocks with a different structure. Figure 4a shows the travel-time curves reduced with the reduction velocity of 8 km/s and converted to the source–receiver midpoint. The envelope of these travel-time curves is the t_0-line for the refracted waves from the boundary with the interface with the boundary velocity 8.0 km/s, the Moho, whereas the travel-time curves of the reflections from this interface are tangential to this envelope at the critical points. The reduced travel-time curves corresponding to the boundaries with velocities ranging from 3.8 to 8.0 km/s are shown in Fig. 4b. These curves delineate three main blocks with the different wave field patterns.

In the southern part of the profile (SPs 0–200 km), the *P*sed phase is tracked up to the offsets of 0–15 km from the shot points, and then the first arrivals show the *P*g wave with the gradually growing apparent velocity of 6.0–6.3 km/s (Fig. 4a). This phase typically dies out at a distance of ~90 km from the source. The next arrivals show an intense wave from the M boundary (*P*mP) with an extended travel-time curve: this phase is typically tracked up to the offsets of 80 to 120 km, and sometimes up to 180 km (Fig. 3a), in which case its apparent velocity is 6.3–6.4 km/s. Within this segment of the profile, the wave refracted from the M boundary, *P*n, is only identified in two seismograms in

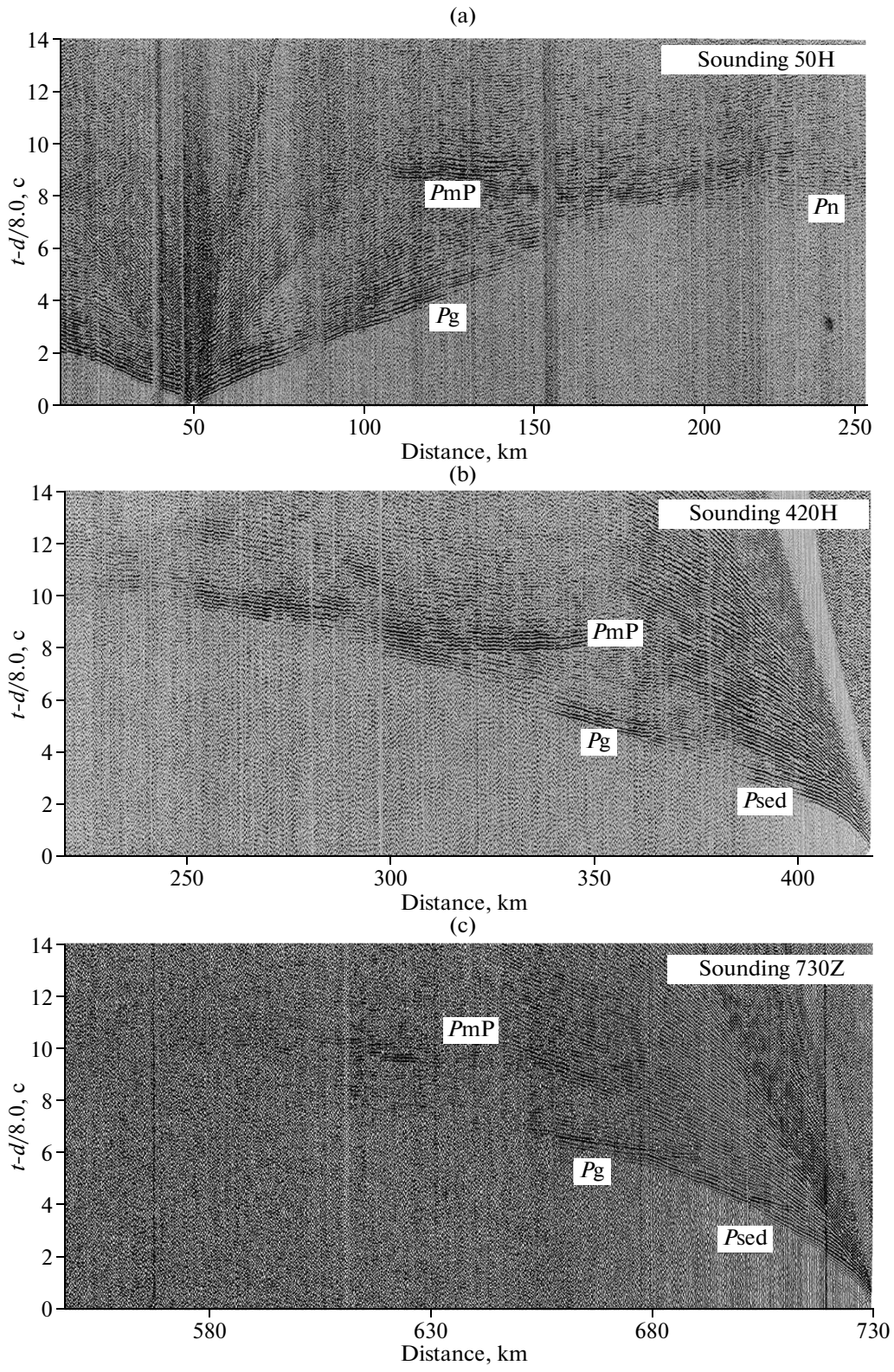

Fig. 3. The record-section of the *P*-wave seismograms obtained on the 1-AP profile at SPs (a), 50; (b), 420, and (c), 750 km. *P*sed are the *P*-waves refracted from the sedimentary cover; *P*g, from the crystalline part of the crust, and *P*n from the top portions of the mantle; *P*mP are the reflected waves from the crustal bottom; the M-boundary; *t* is time; and *d* is the distance from the source to the receiver.

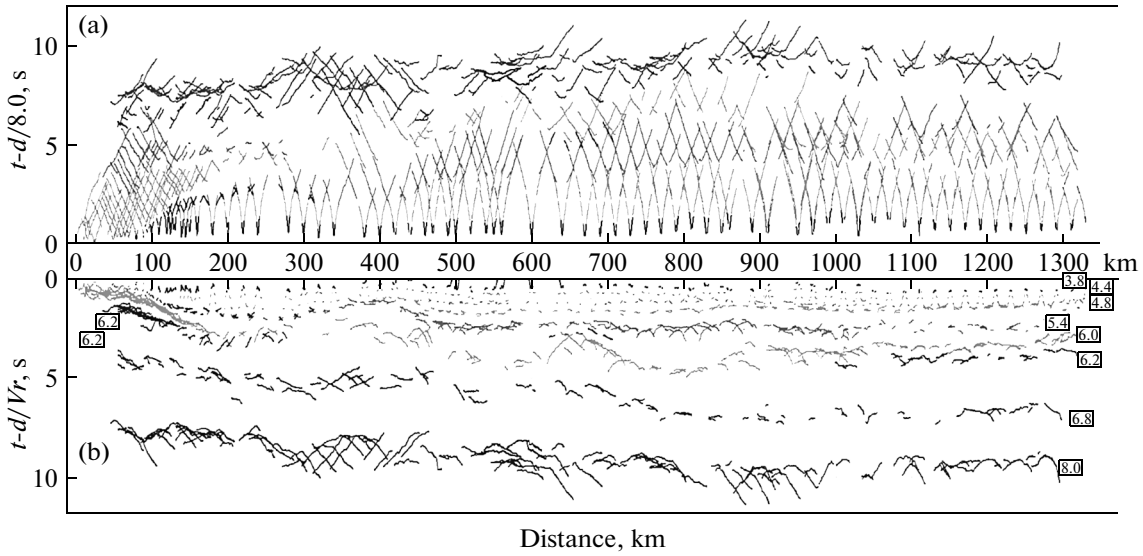

Fig. 4. (a), The observed *P*-wave travel-time curves on the 1-AP profile, reduced with the reduction velocity $Vr = 8.0$ km/s and transformed to the midpoint of the receiver-source distance d; (b), the travel-time curves of the waves from the boundaries with the different boundary velocities, reduced and transformed to the midpoint of the receiver-source distance. The reduction velocities Vr for each group of the travel-time curves correspond to the boundary velocities from 3.8 to 8.0 km/s; the time $t\text{-}d/Vr$ characterizes the values t_0 of the corresponding travel-time curves.

the form of a short small-amplitude event with the apparent velocity of 8.0 km/s.

A different wave pattern is observed in the profile interval of SPs 200–450 km. The *P*sed phase is observed up to an offset of ~20 km, after which the first arrivals come to correspond to the wave with a velocity of 5.7–5.8 km/s. This wave is unlikely to be related to the crystalline crust; at the same time, its velocity is also too high for the sedimentary cover. In the northern segment of this block, this wave with the unclear nature is followed by the *P*g phase with a velocity of 5.8–6.2 km/s, which is observed up to the offsets of 80–90 km. Then the reflections from the boundary in the crystalline crust become the first arrivals with the velocity of 6.3–6.5 km/s. At the offsets of 120–140 km, these waves are changed by the reflections from the Moho. At the center of this block (SP 300 km), the time of recording of the *P*mP phase increases by 1–2 s.

In the profile interval from SP 450 km to SP 500 km, the wave pattern changes, and this change is not gradual but marked with the violation of the correlation between the main phases (Fig. 4a). The *P*sed wave is observed in the first arrivals in the interval from SP 340 to SP 430 km up to an offset about 15 km. Up to the offsets of 80–100 km, the *P*g wave from the basement arrives first with a velocity of 5.8–6.2 km/s. After this, the intense reflections from the intermediate crustal interfaces are observed in the first and secondary arrivals (Fig. 3b). At the 430–450 km SPs, at the offsets of 40–50 km, the correlation of the first phases is broken and the high-velocity (~7.0 km/s) waves are only observed within short intervals at distances of 80–100 km. These waves are typically associated with the local heterogeneities and oblique boundaries. This profile interval is also marked with the violation of the correlation of the *P*mP waves which are then recorded at large times (9–10 s), indicating a steep deepening of the Moho in this region.

At the 500 km SP, the wave pattern stabilized and the *P*mP waves again form a compact group at the traveltimes of 8.2–9.2 s. However, in this interval of the profile (500–600 km SPs), the travel time curves of the crustal waves differ from those described above: the time and region of tracing the *P*sed waves and, correspondingly, the *P*g waves increases (up to 80–100 km from the shot point) and, besides the reflected wave with the apparent velocity of ~6.4 km/s, also the wave whose velocity is above 6.8 km/s, is recorded.

Farther up along the profile, in the interval of the 650–1330 km SPs, the observed wave fields are more stable. The first arrival travel-time curves at the offsets from zero to 90 km are typically approximated by a single curve with the apparent velocity progressively increasing from 3.5 to 5.8 km/s (the *P*sed wave). Then, the *P*g wave from the crystalline crust with 6.0–6.4 km/s is recorded. Very often, the reflection from the sediment bottom from the top of the basement is present. A more precise identification of this wave is impossible due to the small difference in the velocities between the sediments and crystalline crust. The reflections from the Moho within this block form short travel-time curves with an unstable shape (Figs. 3c, 4a). The refracted waves from this interface are weak and rarely recorded.

The identified velocity blocks correspond to the main tectonic structures of the region. The uppermost

block (0–200 km SPs) corresponds to the Kola–Kanin monocline; the central block (200–450 km), to the northwestern margin of the South Barents Basin; and the northern block, to the North Barents Basin. The reduced travel-time curves with different reduction velocities (Fig. 4b) clearly visualize the changes that occur in the travel times of the waves with different velocities and, correspondingly, in the crustal structure in these basins. These changes are not only due to the different thickness of the sediments. Within the North Barents Basin the *P*g waves characterizing the crystalline crust are lower, and the general pattern of the wave field is more stable. The southern part of the profile is characterized by the varying wave pattern which points to the sharp horizontal heterogeneity of the crust.

THE *P*-WAVE PROCESSING TECHNIQUES

The processing and interpretation of the DSS data, just as the data of the other geophysical methods, is fraught with a considerable uncertainty. This is not only due to the common ambiguity of the inverse problem solution for certain types of velocity models or to the limitations of the measurement systems. Another source of ambiguity is associated with the difference in the approaches the interpreters apply for analyzing the wave fields (picking the waves in the seismograms and identifying their nature) and with the use of the different methods for constructing the velocity models.

For reducing the probable ambiguity of the processing and interpretation of the DSS data, even in the case of measurement systems as dense as on the 1-AP line, it is necessary to carry out the detailed analysis of the wave fields, to involve the entire wave field (the waves of the different types and different origin) for constructing the velocity model, and to consider the entire set of the probable models for selecting the most reliable and feasible one, which most adequately accounts for the kinematic and dynamic features of the observed wave fields.

It was noted above that the data on the 1-AP line were processed by different techniques and by experts at different organizations. This allows one to assess the capabilities of each particular method alone and to evaluate the overall reliability of the resulting DSS data.

The geophysicists in Sevmorgeo have developed a multistage technology for processing and interpreting the DSS data starting from uploading the seismic records from SBSS to constructing different seismic models of the Earth's crust and upper mantle (Sakoulina et al., 2003; 2009). These technologies make use of the entire wave field, as well as its kinematic and dynamic characteristics.

The character of the wave filed and the density of the DSS observations are suitable for reconstructing the wave image of the Moho. As noted above, the Moho's reflections in the seismic records from DSS are predominant in the secondary arrivals. They are represented by an intense multiphase group with the apparent velocity of ~8.0 km/s. The length of the group and the structure of its interference record vary along the profile. Based on the Moho reflections recorded in the precritical and postcritical areas, the seismic time section was constructed by the procedure technique similar to the CDP technique: after introducing the kinematic corrections, the seismic records were reduced to the midpoint of the source–receiver interval and then summarized. Figure 2 shows the composite dynamic section constructed for the sedimentary cover (the depth interval from 0 to 30 km) from the CDP reflection data and for the crust/mantle transition zone (depth interval from 30 to 50 km) from the Moho reflections in the DSS seismograms. At places, the dynamical image of the Moho is complicated by the energy bursts associated with the approach of the M-reflected wave by the reflections from the intracrustal interfaces. The low fold of the measurements (3–4) is not always sufficient for suppressing the effects of the intracrustal reflections in the course of processing. Therefore, the M boundary should be considered as the envelope of the signal energy in the seismic section. At the same time, the obtained dynamical section quite adequately reproduces the structural details of the crust and upper mantle.

It is worth noting that at present, the DSS data processing is mainly conducted on the kinematic level, i.e., with the use of travel times (regardless of whether a direct or inverse problem is solved).

In Sevmorgeo, kinematic processing of the data is conducted with the use of the XTomoDPU kinematic data preparation software developed by XGeo Ltd and the Granitsa system of kinematic processing designed in Sevmorgeo. The key result of the first stage of the kinematic processing is the identification of the reference waves (in the form of the their picked arrival times) associated with the extended seismic boundaries; the formation of the systems of the travel-time curves for the waves of the same type (i.e., reflected and/or refracted) corresponding to certain boundaries; and the identification of the first arrivals of the waves.

One of the approaches to wave field analysis consists in constructing the time sections by the reduced travel-time-curve method (Fig. 4). The name of the method corresponds to one of the procedures of constructing the time section: the observed travel-time curves are reduced with different reduction valocity *Vr* and transformed to the midpoint of the shot-point–receiver interval (Pavlenkova, 1979). These transformations provide the analogs of the kinematic time sections t_0 for the seismic boundaries with the boundary velocities equal to the reduction velocities *Vr*. The lines t_0 are formed as the envelopes of the reduced travel-time curves of the first arrivals (refracted waves)

and from the reflected waves' times at the critical points. These transformations for the 1-AP profile were carried out in the Granitsa system. The travel-time curves of the main waves reduced with the boundary velocities of the corresponding interfaces and transformed to the midpoint of the source–receiver interval, with the time axis inversion, are illustrated in Fig. 4b. The time $t\text{-}d/Vr$ characterizes the t_0 values. Despite the (very significant in some cases) scatter of the travel-time curves, which is due to both the inclination of the boundaries and the variations in the boundary velocities along the profile, the "kinematic" time section fairly reliably reflects the overall structure of the crust, the presence or absence of sharp boundaries with certain boundary velocities in it, the character of the variations in the topography of the boundaries, and the ratios of the layers' thicknesses between these boundaries. The obtained time section along the 1-AP profile describes the structure of the boundaries in the sedimentary layer with velocities of 3.8 to 5.4 km/s and the crystalline crust with velocities of 6.0, 6.8, and 8.0 km/s.

In the initial processing and interpretation of the 1-AP DSS data in Sevmorgeo, different approaches to solving the inverse kinematic problem (seismic tomography and direct inversion of the travel-time curves of the reflected and refracted waves) were used for constructing the velocity sections.

The seismic-tomography method which only considers the travel-time curves of the first waves provides the model with a continuous velocity distribution (Ditmar et al., 1993). The method is based on refining the initial velocity model by the optimizing algorithm which minimizes the residuals between the observed and calculated travel times at, generally speaking, small changes in the initial velocity model. With the tomographic method, one may reconstruct the discrete velocity distribution in a given region intersected by seismic rays from the system of the travel-time curves. The results of the reconstructions depend on the initial velocity model.

The seismic tomography velocity section (Fig. 5b) calculated along the 1-AP profile by the Firstomo program (designed by P.G. Ditmar and Yu.V. Roslov in 1997) has a mosaic pattern and represents the crust in a complicated form (Sakoulina et al., 2003; Ivanova et al., 2006). This is due to the fact that the travel-time curves of the first waves that are used for the reconstructions have gaps caused by the absorption or low amplitude of the refracted waves or the appearance of the reflected waves in the visible first arrivals. A stronger averaging of the travel-time curves, with their rarefying, would suppress this mosaicity; however, this would significantly reduce the informativity and reliability of the obtained results.

The seismic-tomography section shown by the lines of equal velocities does not contain direct information about the seismic boundaries and includes a continuous velocity set from the minimal to the maximal values specified in the initial model. Besides, the seismic-tomography section underestimates the velocities (i.e., at a fixed depth the velocity in the tomographic model is lower than the real velocity), and this underestimation increases with depth. However, it should be noted that, despite these shortcomings, the tomographic velocity model reconstructed from the first arrivals travel times generally reveals the key geological structures along the profile. This model provides the first insight into the deep structure of the Earth's crust without much effort on analyzing the wave field.

An alternative approach to solving the inverse kinematic problem lies in the direct inversion of the reflection and refraction travel-times, which provides the velocity estimates and reconstructs the seismic boundaries. The implementation of this approach in the Granitsa system is illustrated in Fig. 5a. The sedimentary section is represented by the one-dimensional velocity columns at the sounding points. Each column is obtained by the layer-by-layer interpretation of the head wave's travel times by the t_0 method in the local layered laterally uniform model of the medium with flat sloping boundaries. The set of the columns provides a coarse but stable approximation to the 2D model. The crustal boundaries including the Moho can be reconstructed from the travel-time curves of the refracted and reflected waves after introducing the kinematic corrections in them.

Thus, based on the solution of the inverse kinematic problem along the 1-AP profile, we have reconstructed the deep section capturing the entire thickness of the crust and identified the main boundaries in the sedimentary cover and crystalline crust. The accuracy of the deep reconstructions depends on the errors in wave discrimination and identifying their origin, as well as on the calculation errors, including those associated with the layer-to-layer recalculation of the kinematic parameters from the top downwards along the section. In the Granitsa system, the sharply contrasting boundaries in the sediments, the basement top, and the Moho are traced most reliably. The reconstruction errors of the boundaries within the crystalline crust are rather big; thus, we can only speak about the velocity characteristics of the corresponding intervals of the sections. The discussed velocity section, in contrast to the tomographic one, may serve as a starting section for the subsequent modeling.

The most complete use of the entire wave field for constructing the seismic section is provided by the mathematical modeling which is as of now the most informative method for interpreting the DSS data (Pavlenkova and Pshenchik, 1982; Roslov et al., 2009; Kashubin et al., 2011; 2013b). This method consists in repeatedly solving the direct problem for certain starting velocity models, comparing the calculated wave characteristics (travel-time curves or synthetic seismograms) with the observed wave fields, and selecting the most reasonable model based on this comparison. This approach enables model construction at each

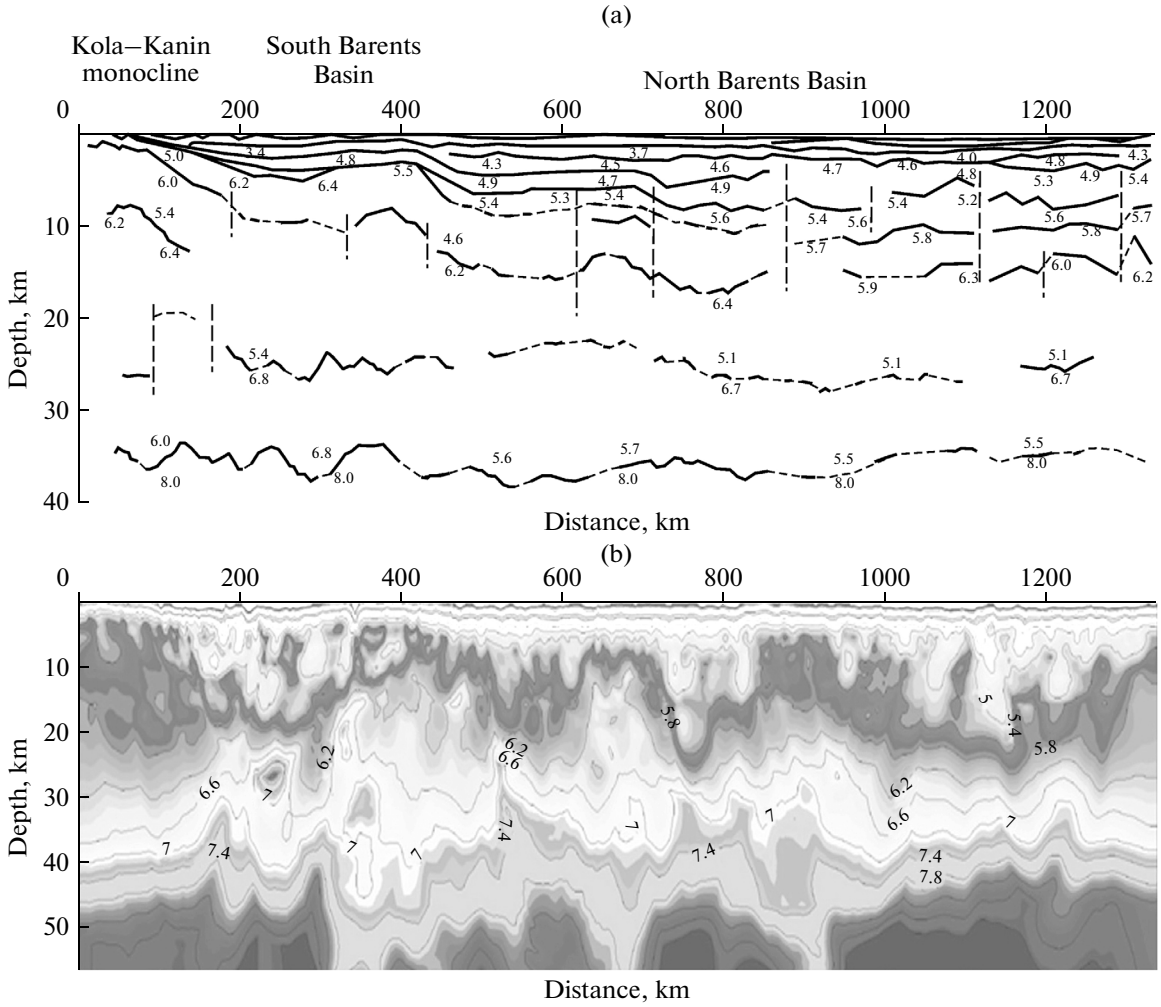

Fig. 5. The seismic sections of the crust along the 1-AP profile constructed (a) in the Granitsa system and (b) by the tomographic method (the velocities in the sections in km/s).

desired complexity level in terms of both the character of the variations in the geometry of the boundaries and in the character of the vertical and lateral changes in the velocities. The mathematical modeling is a process with many feedbacks as a result of which not only the velocity section is constructed but also the probable ambiguity of the reconstruction is evaluated and the nature of the recorded waves identified.

The most programs intended for the solution of the two-dimensional direct problem employ the ray tracing technique (Alekseev and Gel'chinskii, 1959; Červený et al., 1977), and the mathematical modeling is frequently referred to as ray tracing. Simplicity and physical transparence make this method a useful instrument for routine calculations and, most important, for the simultaneous analysis of the wave field. The calculations of the amplitudes of the reflected and refracted waves in this method rely on the assumption that the intensity of the wave is largely determined by the size of the ray tube in the recording region of this wave: the stronger converging rays have lower amplitudes. To this end, the calculations are conducted with equal spacing between the rays at their exit from the source. In these calculations, the amplitude of the refracted wave can be qualitatively assessed even without the amplitude graphs or synthetic seismograms, from the travel-time curves alone, because the size of the ray tube in the wave recording area can be figured out from the density of the points in the calculated travel-time curve.

The ray tracing along the 1-AP profile was conducted by two programs: the SeisWide software, which works under Windows and uses the ray-tracing algorithm previously presented in the RayInvr program product (Zelt and Ellis, 1988) for Linux, and the Seis83 program (Červený and Pšenčík, 1983), which is also designed for Windows. The programs differ by the parameterization of the velocity model; however, their key distinctions are associated with the user interface. In the SeisWide program, the travel-time curves calcu-

lated for the velocity model can be directly superimposed on the initial seismic record; besides, the program facilitates model fitting by simultaneously processing the wave fields from several soundings. In the Seis83 program, a comparison is only possible with the observed travel-time curves. However, the intensity of a given wave can be estimated from the distance between the points of the calculated travel-time curves.

Figure 6 shows the sections constructed in Sevmorgeo with the SeisWide software (the top panel) and in IPE RAS with the Seis83 program (the bottom panel). Both sections share the key features of velocity distribution but differ by the degree of detail. It is worth noting that the distinctions of these models are unrelated to using different software for directly solving the problem.

The reliability and the degree of detail of the reconstruction of the velocity model by the ray-tracing technique are not exclusively determined by the degree of convergence of the calculated and observed fields but also contributed by all the previous steps of the interpretation. The starting model that is closer to the final solution and that contains fewer small details poorly supported by the measurements provides a more reliable solution. For forming the most objective starting model, one should use the maximum possible information provided by the DSS data, including the results of the detailed wave field analysis (on the level of seismograms, travel-time curves, and their various transformations), the velocity sections constructed by the different methods of solving the inverse kinematic problem, and, wherever possible, incorporate additional data, in particular, on the CDP reflections.

We note that the analysis of the wave fields extends to the step of the mathematical modeling. It is only through the numerous calculations of the rays, travel-time curves, and synthetic seismograms for the different versions of the model that we gain an insight into the nature of the recorded waves, reconcile them with the boundaries or layers in the section, and refine their correlation.

The results of the ray tracing also largely depend on the degree of detail specified by the interpreter for fitting a model. Practical experience shows that for obtaining the detailed sections it is reasonable to do the calculations (to solve the direct problem) by successively moving from one shot point (one receiving point in the inverted system offshore) to the next one by fitting all the observed waves and identifying their nature. These general principles of ray-tracing technology were, to a certain degree, implemented by the authors of the sections shown in Fig. 6. The complexity (the degree of detail) of the velocity model is determined by how the local features in the wave field, which constrain the discrimination of the separate bodies and layers with high and low velocities, the construction of the reflecting surface elements with complicated shapes, etc., are treated and factored into the modeling.

The first section (Fig. 6a) provides a more detailed picture of the structure of the sedimentary cover. In particular, a high-velocity layer is identified at a depth of 3–4 km in the southern part of the profile (SPs 100–300 km). However, the section overall has a rather smoothed character and only reflects the key features of the field of the reference waves.

The second section (Fig. 6b) exposes the isolated high-velocity bodies, reflecting surfaces with complex shapes, etc. Particular attention during the modeling was paid to the reflecting boundaries in the crust-to-mantle transition zone which enable the structure of the Moho to be tracked and the regions of the probable dislocations complicated by the local bodies and sloping boundaries.

Figure 7 shows an example demonstrating the possibility of a local intrusion (430–480 km SPs) of rocks with high seismic velocities (6.7 km/s) into the crust. Here, the travel-time curves of the high-velocity *P*-waves (*P*hv) that have been recorded in the first arrivals by the bottom seismic stations are clearly observed at the 420 and 500 SPs. They form a system of the reversed travel-time curves allowing the determination of the shape of the anomalous body and the velocity in it (Fig. 7).

A more objective modeling can be achieved by involving the wave fields in the form of seismic records and travel-time curves. The travel-time comparison on the kinematic level alone may yield additional errors when fitting the model, which are associated with the accuracy of picking the arrival times (i.e., dependent on the results of the picking). At the same time, the discrimination, identification, and correlation of the waves should rather be conducted at the level of the travel-time curves.

The comparison of the resulting sections constructed along the 1-AP profile by the different methods and with the different degree of detail (Figs. 6a and 6b) demonstrates their fairly close convergence in reproducing the key structural features of the crust and uppermost mantle. The sections differ in the details. This concerns the certain local bodies and dislocations along the reflecting boundaries revealed in the crust. The convergence of the sections constructed by the different methods and different interpreters characterizes the general reliability of the DSS reconstructions, i.e., the capabilities of this method. Hence, the application of a variety of methods for the interpretation of the DSS data gives a reliable estimate of the validity of the resulting velocity models and ensures identification of the model segments or particular details where the reconstructions are ambiguous.

For assessing the general capabilities of DSS, it was instructive to compare the described reconstructions with the results of the DSS-76 studies that were previously conducted in the southern part of the 1-AP pro-

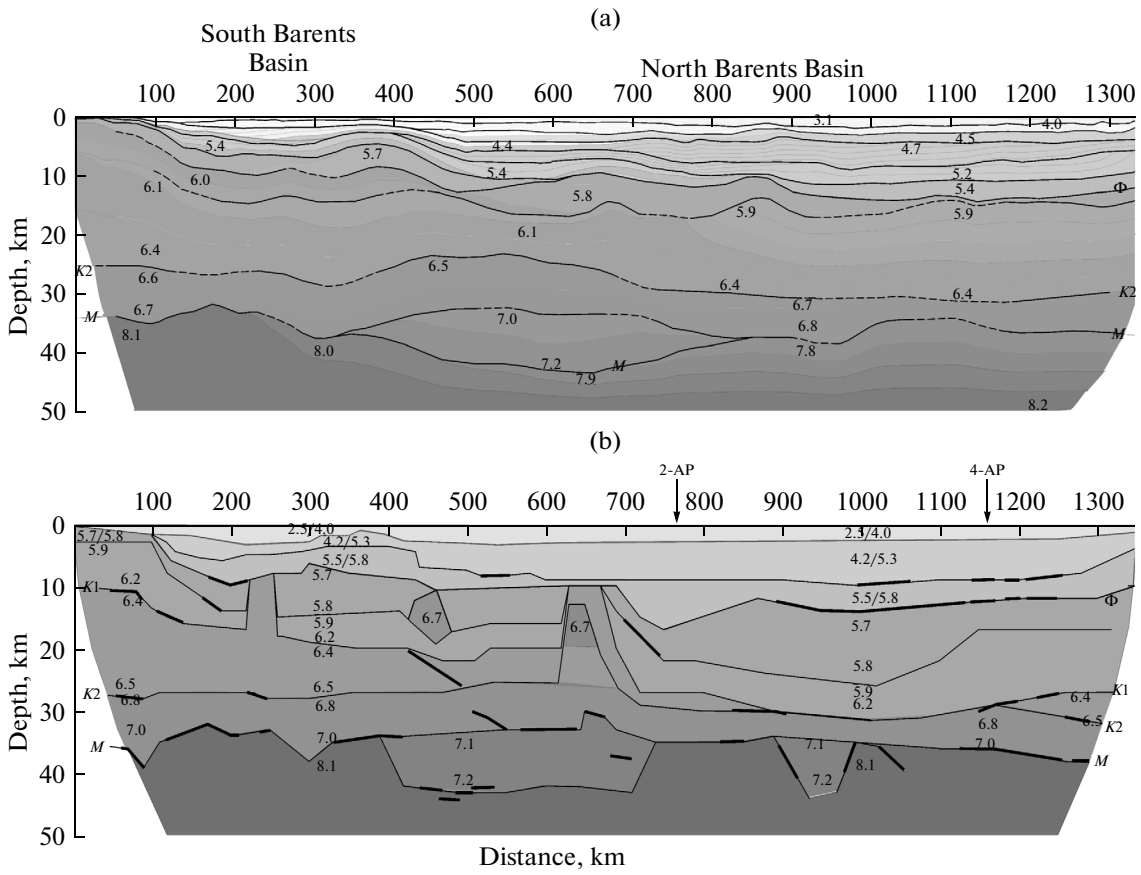

Fig. 6. The seismic sections of the crust along the 1-AP profile constructed by the ray tracing technology: (a) in Sevmorgeo with the aid of the SeisWide software; (b) in IPE RAS by the Seis83 software (the reflecting boundaries in this section are shown by the thick lines).

file. These have been the first works in the Barents Sea that were conducted with the bottom stations and explosions (Davidova et al., 1985; Davidova and Mikhota, 1986). The measurement setup was less detailed (with a spacing of 30–40 km between the bottom stations); however, all the reference waves described above were traced fairly confidently. Besides, excitation of the seismic signals by explosions instead of air-gun shots enabled a more reliable tracing of the *P*n refractions from the M-boundary.

The DSS-76 data were processed by a set of methods that were accepted at that time. They were dominated by the technique developed for head waves, which formed the basis for the DSS technology (Gamburtsev et al., 1952). However, also the interpretation methods for the refracted and reflected waves were simultaneously developing at that time. As a result, several versions of the section along the DSS-76 profile were obtained. The most comprehensive reconstructions were conducted by solving the one-dimensional and two-dimensional inverse problems for the velocity section and by the graphical reconstructions of the time fields of the basement surface, M-boundary, and separate reflecting surface elements (Fig. 8a) (Davidova and Mikhota, 1986). The velocity model in the form of the velocity contours was also constructed by the method of reduced travel-time curves (Pavlenkova, 1986); this model generally fairly well agrees with the model in Fig. 8a. The third version of the section was obtained by the method for the head waves (Tulina, 1986): based on the composite time-distance plots composed of the reversed and overlapping travel-time curves, several refracting boundaries with the varying boundary velocity were constructed (Fig. 8b). By comparing Figs. 6b and 8, one may see that the section shown in Fig. 8b fairly well agrees with the detailed reconstructions along the 1-AP profile described above. Even such a complicated structure of the crust with the high-velocity inclusions in its middle part has been noted as early as in the DSS studies in 1976. As far as the reconstruction in Fig. 8b is concerned, this section is difficult to correlate to the other model reconstructions (Figs. 5 and 6): it demonstrates seismic boundaries of an unclear nature which are barely helpful even in tracking the top of the basement. This means that the head-wave method is only efficient in reconstructing the sharply contrasting refracting boundaries, i.e., in the reconstructions of the sed-

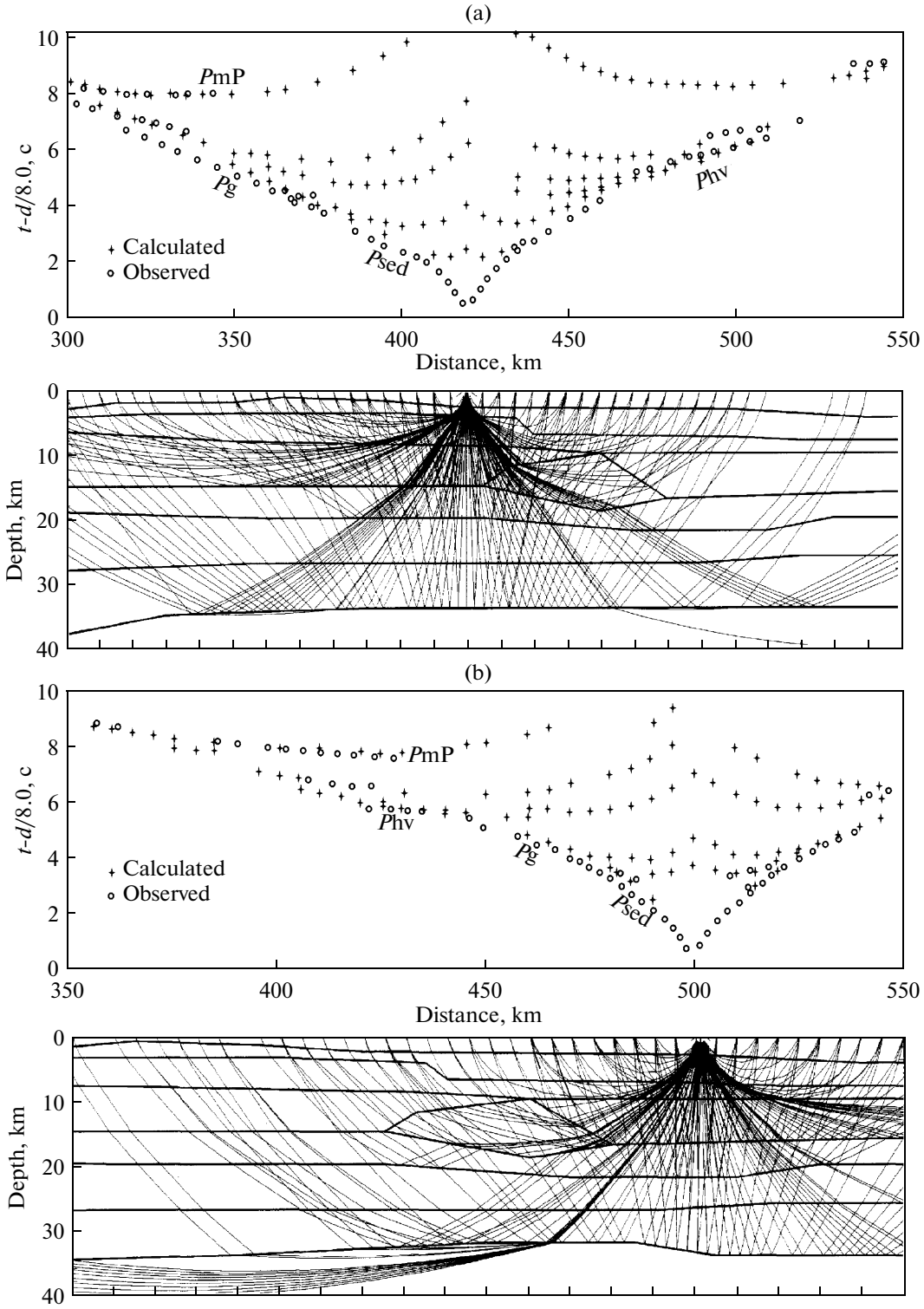

Fig. 7. The comparison of the observed and calculated travel-time curves and the ray schemes for the bottom stations at the 1-AP SPs 420 and 500, which model the local high-velocity body in the crystalline crust (Fig. 6b). *P*hv are the high-velocity waves; the designations of the other waves are presented in Fig. 3.

imentary cover. For exploring the environments with low velocity gradients such as, e.g., the crystalline crust, this method is inefficient.

Generally, the comparison of the reconstructed sections on the 1-AP profile attests to the sufficiently high reliability of the revealed vertical and lateral variations in the velocity and the structure of the basic boundaries in the crust if the entire wave field and a variety of interpretation methods for all wave types were used for the reconstructions.

PROCESSING THE *S*-WAVE FIELD

The deep seismic studies in the continental regions have been informative concerning the DSS data not only for *P*-waves but also for *S*-waves. The latter can be used for complementing the structural reconstructions by the more detailed data about the composition and mechanical properties (absorption and velocity anisotropy) of the crustal material. The results of these studies for different regions have been published in (Egorkin et al., 1981; Aleinikov et al., 1986; 1991; Krylov et al., 1991; Kashubin et al., 1991; 1997; 2001). The offshore studies typically have not explored the *S*-waves. In (Lukashin et al., 2003; Kashubin et al., 2013b) it was shown that even the *S*- (converted) waves can also be studied in the marine DSS with bottom stations.

The analysis of the three-component records obtained during the offshore DSS measurements with SBSS shows that, along with the compression-wave field, which is most distinctly manifest in the records from hydrophones and in the vertical components, the horizontal components are ubiquitously recording quite intense waves with the kinematic characteristics corresponding to the shear and converted waves (Kashubin et al., 2013b). Since the marine seismic measurements are conducted with the air-gun sources placed at a depth of 20–30 m in the water layer and, correspondingly, only generating the *P*-waves, all the non-*P*-type waves recorded by the bottom station are, in fact, converted since within a part of their path from the source to the receiver they propagate as *P*-waves. Besides, the presence of the sharp acoustic boundary—the sea bottom, which is both an interface of the liquid and solid phases and a highly-contrasting velocity boundary—leads to the formation of the intense multiple waves associated with this interface.

The multicomponent processing of the 1-AP data was carried out in VSEGEI for the southernmost 300–km segment of the profile. The examples of *S*-waves recorded on this interval are shown in Fig. 9. The analogs of the *P*g and *P*mP reference *P*-waves, which are predominantly recorded in the horizontal components—*S*g and *S*mS—are the most clearly pronounced *S*-waves. However, the *S*-waves are identified in the seismograms far less reliably than the *P*-waves (Fig. 9). In the visualized horizontal components of a seismic record in the corresponding reductions, the shear analogs of the compression waves are identified in ~30% of the cases.

Recently, the geophysicists at VSEGEI have developed a method that is capable of routinely identifying *S*-waves in the marine DSS data (Kashubin et al., 2013b). This method offers several options for processing the multicomponent records. For highlighting the *S*-waves in the records in the secondary arrivals, the following procedures are conducted: (1) transformation of the records of the fixed *X*- and *Y*-components into the records of the tracking components: radial *R* and transversal *T*; (2) highlighting the shear waves by suppressing the compression waves in the area of first arrivals and the wave train of multiple waves with the apparent velocities close to the *P*-velocities. This processing of the measurement data significantly improved the records of the *S*-waves and allowed us to track all the main waves necessary for constructing the velocity model along the selected segment of the profile.

As noted above, the wave fields of the *P*- and *S*-waves recorded on the 1-AP profile are generally similar and, hence, they can be interpreted within the same seismic section geometry. For more objectivity, joint processing by a common procedure was carried out for the *S*- and *P*-waves within this segment. The ray tracing was conducted with the use of the SeisWide and Seis83 software. The modeling covered the refracted and reflected waves. The correction of the model was conducted manually by changing the velocities, depth, and geometry of the boundaries in the area illuminated by the rays from the corresponding shot–receiver points. The direct problem solution procedure was repeated each time after the correction of the model for all observation points until a reasonably close agreement between the calculated and observed travel-time curves was achieved.

Primarily, the *P*-velocity section was constructed, and then, the *S*-velocity section with the same geometry was fitted. To this end, the *P*-velocities were converted into the *S*-velocities by multiplying by 1.73. In the upper part of the section, the Vp/Vs ratio estimated by the interpretation of the converted waves was used. Then, the Vs values were interactively adjusted without changing the geometry of the section until the calculated travel-time curves of the refracted and reflected *S*-waves became reasonably close to the observed wave fields in the horizontal components.

The results of this processing are illustrated in Fig. 10. The lower crust is characterized by a thickness of ~10 km and *P*-velocities $Vp = 6.8–7.1$ km/s. The thickness of the middle crust within this part of the profile varies quite significantly (from 7 to 17 km). The middle-crustal *P*-velocities are $Vp = 6.4–6.6$ km/s and the velocity ratio is $Vp/Vs = 1.73–1.78$. The upper crust has *P*-velocities of 6.0–6.3 km/s, $Vp/Vs = 1.73–1.75$. Its thickness varies from one to ten km, and its top boundary deepens from almost the surface in the coastal part of the profile to a depth of 12 km at the end of the profile segment. Within the profile interval of

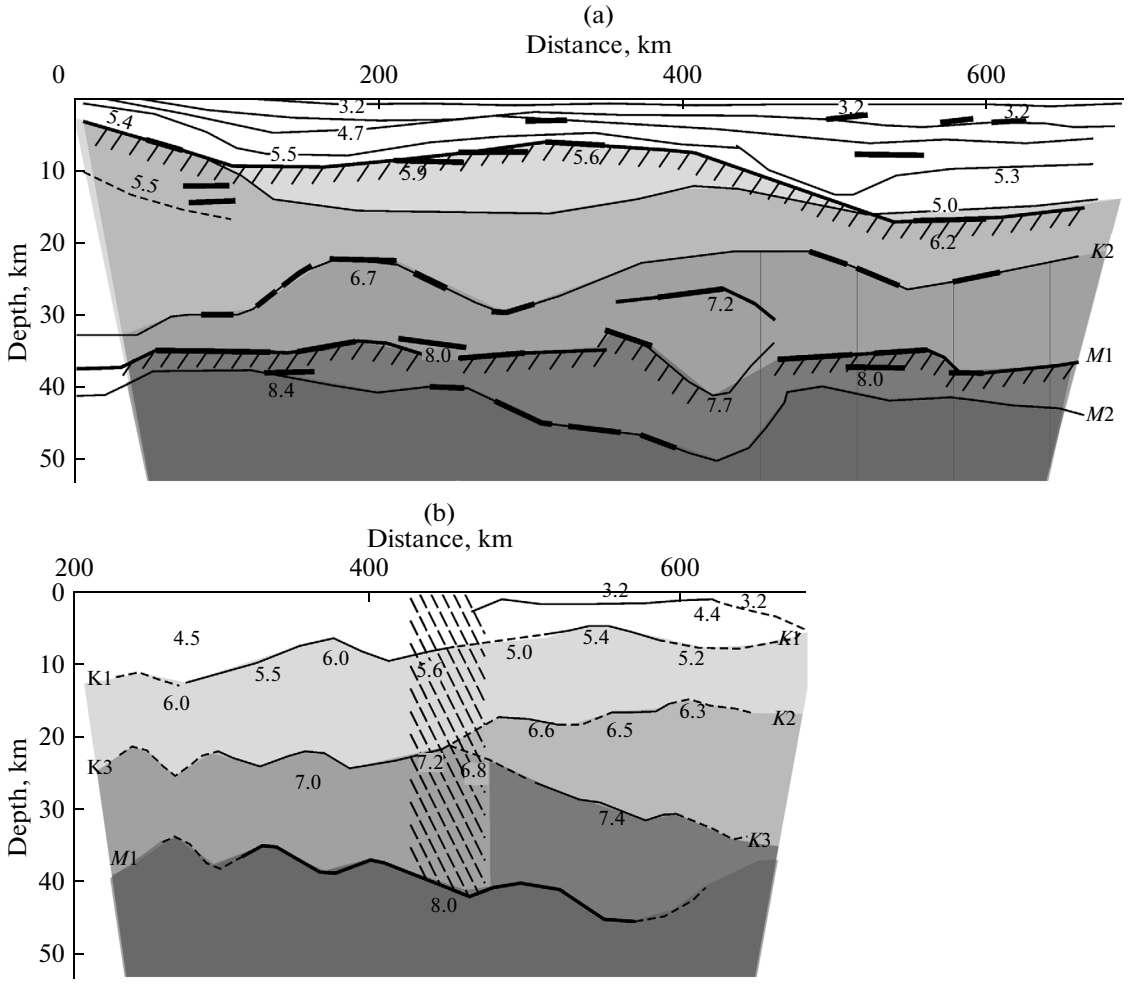

Fig. 8. The crustal sections constructed along the DSS-76 profile coinciding with the southern part of the 1-AP profile according to the data (a) (Davidova and Mikhota, 1986); (b) (Tulina, 1986).

the 220–240 km SPs, the upper crust is intruded by the high-velocity body from the middle crust.

The thick sedimentary cover is represented by several layers with *Vp* varying from 3.0 to 5.3(–5.9?) km/s; $Vp/Vs = 2.2–2.5$, and the thickness increasing with the distance from the land-sea boundary. The obtained results of processing the *S*-wave field along the 1-AP profile agree with the *P*- to *S*-velocity ratio data estimated for the neighboring Baltic shield (Janik et al., 2007). This is the important result of the described works which confirm the continental type of the crust in this shelf zone of Eurasia.

THE KEY FEATURES OF THE CRUSTAL STRUCTURE ALONG THE 1-AP PROFILE

The combined seismic CDP-DSS studies conducted on the 1-AP profile with the dense measurement system enabled the crustal structure of the Barents Sea from the continent to 1330 km off the shore to be explored with a high degree of detail (Fig. 1). The profile crosses a number of structural features, the main ones being the Kola-Kanin monocline (SPs 0–100 km, Fig. 6), the western margin of the South Barents Basin, and the North Barents Basin (*Barentsevskaya* ..., 1988; Verba, 2008; Verba and Matveev, 2000). As was shown by the seismic studies, these structures significantly differ by the structure of the sedimentary cover and the crust overall.

The Kola-Kanin monocline retains the key features of the Baltic shield crust but with a smaller crustal thickness which is 35 km here versus 40–45 km in the northern part of the shield (Isanina et al., 2000; Pavlenkova, 2006). The sedimentary cover is almost absent here, and the crust is represented by three main layers of the continental crustal pattern with the velocities of 5.7–6.2 km/s in the depth interval from 0 to 10 km (upper crust), 6.4–6.5 km/s at 10–27 km (middle crust), and 6.8–7.0 km/s in the lower crust.

The crust of the western margin of the South Barents Basin (SPs 100–700 km) features a complicated structure. The sedimentary layer's thickness increases

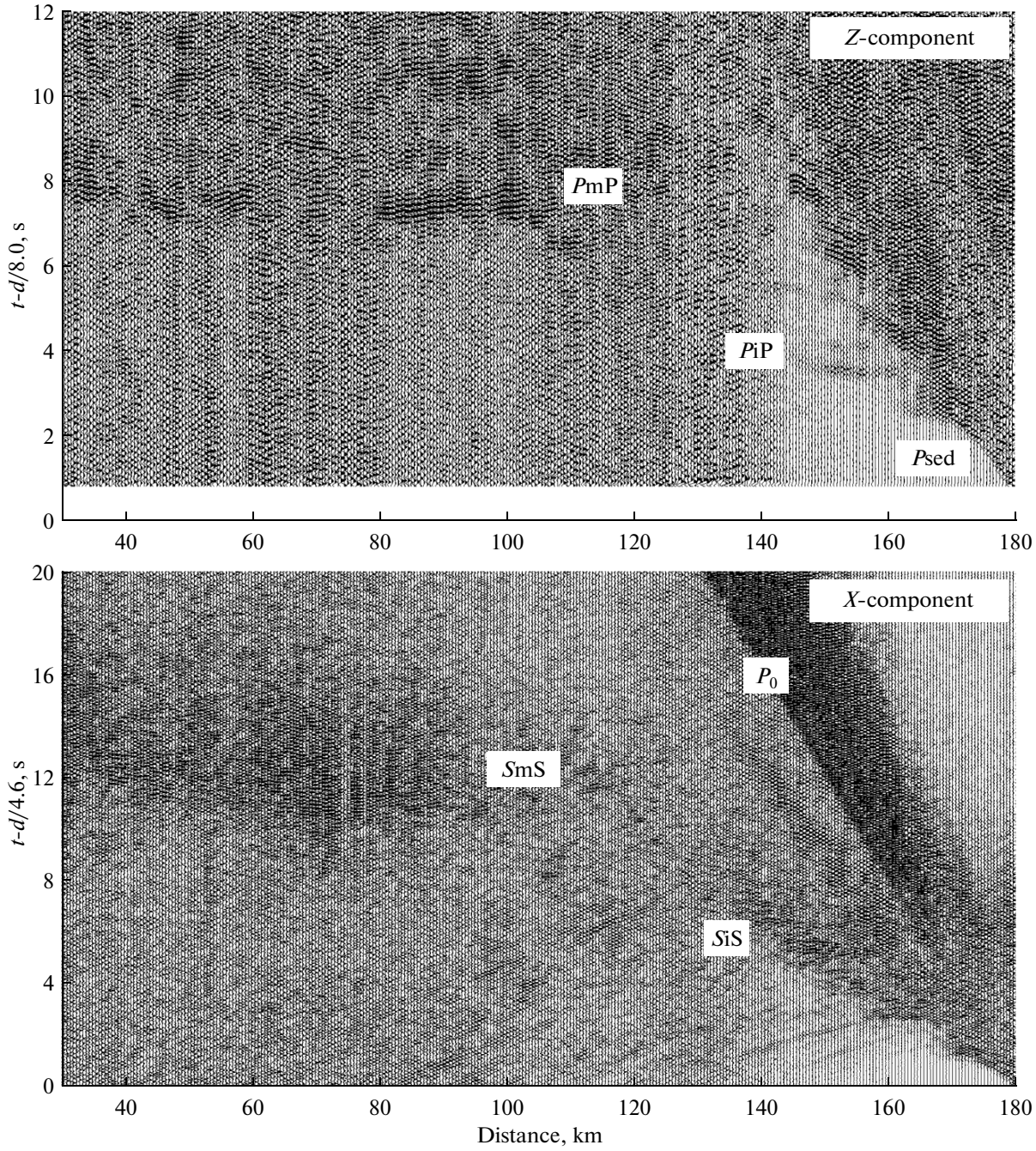

Fig. 9. The stack of the seismograms with the records of the *P*- and *S*-waves at SP 180 km. *P*iP and *S*iS are the reflected *P*- and *S*-waves from the crustal boundaries; *P*mP and *S*mS are the Moho reflections.

here up to 8–12 km. Within this layer, the CDP and DSS data identify several uplifts with the steep slopes (the Fedynskii High, Demidov Aulacogen, and Fersman High). The crystalline crust within this block is also complexly structured. In its upper part, the velocities generally decrease due to the steep reduction of the midcrustal thickness to 7–8 km. However, this overall decreasing trend is interrupted by the high-velocity (6.4–6.8 km/s) intrusions into the upper crust within the profile intervals of the 230–260, 420–470, and 620–670 km SPs (Fig. 6b). These intrusions are correlated to the complications in the sedimentary cover and are the main distinctive feature of the crustal structure of the South Barents Basin compared to the North Barents Basin.

The structure of the lower crust and the Moho in the region of the South Barents Basin is also highly differentiated. At the 400 km SP there is a break in track-

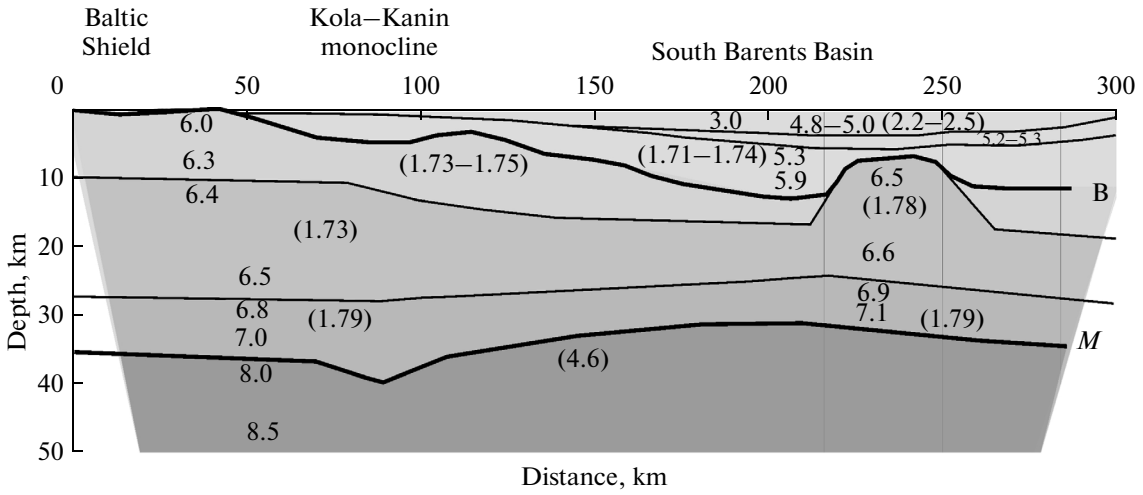

Fig. 10. The velocity section in the *P*- and *S*-waves for the southern part of the 1-AP profile. The section shows the *P*-velocities (in km/s) and velocity ratios *Vp*/*Vs* (in the parentheses). The basement surface (*B*) and the Moho are indicated by the thick lines.

ing the Moho, after which this boundary steeply deepens from a depth of 35 to 43 km. The wave pattern in this area is shown in Fig. 4. However, above the Moho in this part of the profile there is a reflecting boundary at a depth of 30–32 km, which also produces intense reflections which are commensurate with the *P*mP-waves. In the wave portrait of the crust-to-mantle transition zone (Fig. 2), it is this boundary but not the Moho that produces a clearly expressed bulge. The layer velocity between these boundaries is 7.1–7.2 km/s, which is higher than the lower crustal velocities characteristic of this profile but quite typical of the crust of the East European Platform. This high-velocity lower crustal block breaks off at the 700 km SP. It is worth noting that a similar abrupt drop of the depth to the Moho and an increase in the velocities in the bottom portions of the crust are also noted in the Baltic Shield (Pavlenkova, 2006). This Baltic block is significantly larger than its South Barents counterpart and the drop in the depths to the Moho boundary reaches 20 km, whereas the velocity in the bottom part of the crust is 7.3–7.5 km/s. However, this corresponds to the higher average values of these parameters within the shield; i.e., the formation mechanism of such blocks along the M-boundary can be identical within the shield and on the young Barents plate.

At the same 700 km SP, the structure of the Earth's crust also undergoes an overall change which can be associated with the transition from the South Barents to the North Barents basins. Here, the thickness of the sedimentary cover increases insignificantly; the most important change consists in the transformation of the internal structure of the crystalline crust. Within the southern part of the profile up to SP 700 km, the basement is represented by an intense reflector with a complicated topography. In the northern part, the basement deepens and then is almost untraceable by the precritical reflections (the CDP section, Fig. 2). In contrast, in the DSS profile (Fig. 6b), a distinct reflecting horizon is revealed at a depth of 12–15 km within the profile segment of SPs 900–1260 km. This horizon is identified with the basement surface. However, the boundary velocity along this horizon is as low as 5.7 km/s. Low seismic velocities are also characteristic of the entire crystalline crust of the North Barents basin where they are 5.7–6.2 at depths from 15 to 30 km, and the midcrustal layer with velocities of 6.4–6.5 km/s is practically absent in this area.

The anomalously low velocities obtained for the crystalline crust of the North Barents basin are consistent with the DSS data on the 4-AP profile (Sakoulina et al., 2015). These data confirm the fundamental difference in the structure of the Earth's crust in the South Barents and North Barents basins. The untypical structure of the crust within the South Barents basin has been revealed earlier based on the DSS-82 profile data (Fig. 1). The depth of the basin along this profile is about 20 km, whereas the crystalline crust is almost completely composed of the basite material with seismic velocities above 7.0 km/s (Morozova et al., 1995). In contrast, the crystalline crust of the North Barents Basin is distinguished by anomalously low velocities even compared to the normal continental crust. This testifies to the significant difference in the history of the formation of these basins which were previously considered by many researchers as a single depression of probably rifting origin (*Barentsevskaya* ..., 1988; Gramberg, 1997; Verba and Matveev, 2000; Verba, 2008).

CONCLUSIONS AND KEY RESULTS

The deep seismic studies carried out on the 1-AP profile promoted the solution of several tasks important from both the practical and fundamental standpoints. These are the problems of the future develop-

ment of the methods for the marine seismic studies of the Earth's crust and upper mantle and the study of the processes of the general geological evolution of the continental margins.

From the methodical standpoint, the discussed works exhibited fairly promising prospects of applying exactly the combined seismic studies, including the *S*-wave DSS, for exploring the structure of the crust. The suggested technique for processing the three-component records of the bottom stations has demonstrated the possibility of recording, in the form of converted waves, the reference refracted and reflected *S*-waves from the main crustal boundaries and, thus, obtaining the important additional information on the *P*- to *S*-velocity ratio, i.e., on the composition of the crustal material and its mechanical properties.

Another important methodical outcome of the studies on the 1-AP profile consists in the assessment of the capabilities of the different methods for processing and interpreting the marine DSS data. The data processing for this profile carried out by different organizations with the use of a variety of wave field analysis methods and different software for the solution of direct and inverse problems confirmed the highest informativity and reliability of the velocity model reconstructions based on the mathematical (ray tracing) modeling. Here, it is shown that the comprehensive analysis of the wave fields at all stages of the modeling, identification of seismic phases, and involvement of the entire information for these waves are critical for the efficiency of ray tracing. The selection of the most reliable initial model based on the wave field analysis and construction of the velocity models by different methods is an important stage of the modeling.

The studies carried out on the 1-AP profile are also of great value for the solution of a number of the key geodynamical problems, e.g., concerning the formation of the deep troughs and different crustal types. In this context, the Arctic shelf zones, just as the entire Arctic basin, are of particular interest since they have an untypical crustal structure compared to the other oceanic regions.

The data concerning the geological structure, tectonics, magmatism, and evolution history of the region are summarized in (*Barentsevskaya* ..., 1988; Gramberg and Pogrebitskii, 1993; Verba, 2008; Barrére et al., 2009; Kashubin et al., 2013a). In contrast to the other oceans, the typical oceanic crust with a thickness of less than 10 km and average velocity of 6.5–7.0 km in the Arctic region is only observed in a narrow zone of the midoceanic ridge; most of the area of the ocean is represented by a crust with a thickness of 25–35 km, typical of the continents. However, the interior structure of this crust differs from the continental one by the high velocities in the middle crust and small thickness of the granite-gneiss layer (~5 km); Whether this crust is primary or has been formed as a result of the basification of the continental crust by the mantle melts is still unclear.

The works in the Kara–Barents Sea have not only approved the large thickness of the Earth's crust within this shelf zone but also demonstrated the true continental type of its crust with a thick granite-gneiss layer (the upper crustal layer with *P*-velocities of 5.8–6.4 km/s and velocity ratio $Vp/Vs = 1.73–1.75$, Figs. 6 and 10). In this context, the obtained *S*-velocity data matter significantly: they enable a more accurate estimate of the crustal composition and support its similarity with the crust of the neighboring Baltic Shield: the same seismic parameters of the crust are characteristic of the region of the Kola superdeep borehole (Isanina et al., 2000) and, generally, for the Baltic Shield overall (Pavlenkova, 2006; Janik et al., 2007).

The presence of the deep basins filled with the 15–20-km sediments (Fig. 1) is another peculiar feature of the Barents–Kara shelf. The crustal structure in these basins is fundamentally different which testifies to the different nature of their formation. The crystalline crust of the South Barents basin is composed of basic rocks with seismic velocities of ~7.0 km/s, as established for the DSS-82 profile (Morozova et al., 1995). In the region of this basin on the 1-AP profile, blocks with similar high velocities are revealed in the middle crust (Fig. 6b). In contrast, the crust of the North Barents basin is mainly granite-gneiss: the velocities of ~5.8–6.4 km/s are observed in the crystalline crust up to a depth of 30 km (Fig. 6). The South Kara basin has intermediate velocities of 6.2–6.7 km/s in the upper and middle parts of the crystalline crust (Sakoulina et al., 2009; Roslov et al., 2009).

The formation of the deep basins within the continental margins, particularly, the basins with the high-velocity crust (such as in the South Barents basin) are commonly thought of as related to the rifting processes. The origin of the extended trough in the Barents Sea, which stretches along the Novaya Zemlya Range (Fig. 1), could also be attributed to such processes (Gramberg, 1997; Erinchek et al., 2000; Verba, 2008). However, the deep seismic soundings have shown that the formation of the deep basins in this region contributed to a variety of the processes, among which the key role is played by the transformations of the crustal material (basification and eclogitization of the crust). At the same time, this does not depreciate the importance of rifting in this region, which provides the inflow of the mantle material and thermal energy into the crust.

REFERENCES

Aleinikov, A.L., Nemzorov, N.I., and Khalevin, N.I., *Mnogovolnovaya seismika pri izuchenii nedr rudnykh raionov* (Multiwave Seismics in the Study of the Earth's Interior in Ore-Bearing Regions), Moscow: Nauka, 1986.

Aleinikov, A.L., Nemzorov, N.I., and Kashubin, S.N., The method for identifying the type of the rock from seismic data, USSR Inventor's Certificate no. 1642416 A1 cl. G 01 V1/30, 1991 (unpublished).

Alekseev, A.S. and Gel'chinskii, B.Ya., On the ray method for wave field calculations in the case of heterogeneous medium with curvilinear boundaries, in *Voprosy dinamicheskoi teopii pasppostpaneniya seismicheskikh voln. T. 3* (The Questions of Dynamic Theory of Seismic Wave Propagation. Vol. 3), Leningrad: LGU, 1959, pp. 11–37.

Barentsevskaya shel'fovaya plita (The Barents Shelf Plate), Gramberg, I.S., Ed., Leningrad: Nedra, 1988.

Barrére, C., Ebbing, J., and Gernigon, L., Offshore prolongation of Caledonian structures and basement characterisation in the western Barents Sea from geophysical modeling, *Tectonophysics*, 2009, vol. 470, nos. 1–2, pp. 71–88.

Červený, V., Molotkov, I., and Pšenčík, I., *Ray Method in Seismology*, Prague: Charles Univ., 1977.

Červený, V. and Pšenčík, I., SEIS 83-numerical modelling of seismic wave fields in 2-D laterally varying layered structure by the ray method, in *Documentation of Earthquake Algorithms*, Engdahl, E.R., Ed., Boulder: World Data Center (A) for Solid Earth Geophysics, 1983, Rep. SE-35, pp. 36–40.

Davidova, N.I., Pavlenkova, N.I., Tulina, Ju.V., and Zverev, S.M., Crustal structure of the barents sea from seismic data, *Tectonophysics*, 1985, vol. 114, nos. 1–4, pp. 213–231.

Davydova, N.I. and Mikhota, G.G., The deep structure of the southeastern Barents Sea according to DSS data, in *Izuchenie glubinnogo stroeniya vostochnoi chasti Baltiiskogo shchita i prilegayushchikh akvatorii seismicheskimi metodami* (Seismic Studies of the Deep Structure of the Eastern Baltic Shield and Neighboring Marine Territories), Apatity: AN SSSR, 1986, pp. 70–78.

Ditmar, P.G. and Roslov, Yu.V., Nonlinear tomographic processing of seismic data, *Mezhdunarodnaya geofizicheskaya konferentsiya SEG-EAGO, 1993. Moskva 93. Sbornik referatov* (Int. Geophys. Conf. SEG-EAGO Moscow 93. Collection of Abstracts), Moscow: 1993, Report S.7.8, p. 55.

Egorkin, A.V., Kun, V.V., and Chernyshev, N.M., *P*- and *S*-wave absorption in the crust and upper mantle of the West Siberian Plate and Siberian Platform, *Izv. Akad. Nauk SSSR, Fiz. Zemli*, 1981, no. 2, pp. 37–50.

Erinchek, Yu.M., Verba, M.L., and Mil'shtein, E.D., The concept of the study of the deep structure of the lithosphere in Russia, *Reg. Geol. Metallogen.*, 2000, no. 12, pp. 68–72.

Gamburtsev, G.A., Riznichenko, Yu.V., Berzon, I.S., Epinat'eva, A.M., and Karus, E.I., *Korrelyatsionnyi metod prelomlennykh voln* (Refracted Wave Correlation Method), Moscow: AN SSSP, 1952.

Gramberg, I.S. and Pogrebitskii, Yu.V., The geodinamic system, deep structure, and structural evolution of the Arctic Ocean, in *Evolyutsiya geologicheskikh protsessov v istorii Zemli* (Evolution of Geological Processes in the History of the Earth), Moscow: Nauka, 1993, pp. 146–158.

Gramberg, I.S., The Barents Sea Permo–Triassic paleorift and its importance to the problem of oil and gas potential of the Barents–Kara platform, *Dokl. Earth Sci.*, 1997, vol. 353, no. 2, p. 198–200.

Isanina, E.V., Verba, M.L., Ivanova, N.M., Kazansky, V.I., and Sharov, N.V., Deep structure and seismogeological boundaries of the Pechenga district in the Baltic Shield and the adjacent part of the Barents Sea shelf plate, *Geol. Ore. Deposits,* 2000, vol. 42, no. 5, pp. 429–439.

Ivanova, N.M., Sakoulina, T.S., and Roslov, Yu.V., Deep seismic investigation across the Barents–Kara region and Novozemelskiy fold belt (Arctic shelf), *Tectonophysics*, 2006, vol. 420, nos. 1–2, pp. 123–140.

Janik, T., Kozlovskaya, E., and Yliniemi, J., Crust-mantle boundary in the central Fennoscandian shield: constraints from wide-angle *P*- and *S*-wave velocity models and new results of reflection profiling in Finland, *J. Geophys. Res.,* 2007, vol. 112, pp. 1–28, B04302.

Kashubin, S.N., Experimental data on seismic anisotropy of the crust of the Urals and its probable relation to the oriented fracturing and stress state of the medium, in *Stroenie i geodinamika zemnoi kory i verkhnei mantii* (The Structure and Geodynamics of the Earth's Crust and Upper Mantle), Moscow: GIN AN SSSP, 1991, pp. 29–37.

Kashubin, S., Seismic anisotropy of the upper mantle of the Urals, in *Upper Mantle Heterogeneities from Active and Passive Seismology*, Fuchs, K., Ed., Dordrecht: Kluwer, 1997, pp. 317–324.

Kashubin, S.N., *Seismicheskaya anizotropiya i eksperimenty po ee izucheniyu na Urale i Vostochno-Evropeiskoi platforme* (Seismic Anisotropy and the Experiments on Its Study in the Urals and East European Platform), Yekaterinburg: UrO RAN, 2001.

Kashubin, S.N., Sakulina, T.S., Pavlenkova, N.I., and Lukashin, Yu.P., Characteristics of compressional and shear waves generated in marine deep seismic studies, *Tekhnol. Seismorazved.*, 2011, no. 4, pp. 88–102.

Kashubin, S.N., Pavlenkova, N.I., Petrov, O.V., Mil'shtein, E.D., Shokal'skii, S.P., and Erinchek, Yu.M., The types of the Earth's crust in Circumpolar Arctic, *Reg. Geol. Metallogen.*, 2013a, no. 55, pp. 5–20.

Kashubin, S.N., Sakulina, T.S., Lukashin, Yu.P., and Pavlenkova, N.I., Modern methods for conducting and interpretation and deep seismic soundings in the marginal seas of Russia, in *Aktual'nost' idei G.A. Gamburtseva v XXI veke* (Topicality of G.A. Gamburtsev's Ideas in the 21st Century), Moscow: Yanus-K, 2013b, pp. 175–194.

Krylov, S.V., Seleznev, V.S., Solov'ev, V.M., Suvorov, V.D., and Nikitenko, A.B., Shear waves and seismic anisotropy of the Earth's crust in western Yakutia, *Izv. Akad. Nauk SSSR, Fiz. Zemli*, 1991, no. 2, pp. 26–33.

Lukashin, Yu.P., Semenov, V.P., and Ronin, A.L., Application of multiwave seismics in the marine regional studies, *Razved. Okhr. Nedr*, 2003, no. 4, pp. 7–11.

Matveev, Yu.I., Verba, M.L, Lipilin, A.V., Roslov, Yu.V., and Erinchek, Yu.M, The key results of the decade-long regional combined geophysical studies on the Barents and Kara shelf, *Razved. Okhr. Nedr*, 2005, no. 1, pp. 3–6.

Morozova, E.A., Pavlenkova, N.I., and Herbst, R., Seismic model of the Earth's crust in the southeastern Barents Sea and the problems of ambiguity of its construction, *Fiz. Zemli*, 1995, no. 2, pp. 73–83.

Pavlenkova, N.I., The reduced travel-time curves method and mathematical modeling, in *Obratnye kinematicheskie zadachi vzryvnoi seismologii* (Inverse Kinematical Problems of Explosion Seismology), Moscow: Nauka, 1979, pp. 107–123.

Pavlenkova, N.I. and Pshenchik, I., Mathematical modeling in the solution of two-dimensional inverse problem in DSS, *Fiz. Zemli*, 1982, no. 2, pp. 12–22.

Pavlenkova, N.I., Comparison of the different versions of the section along the DSS profile in the Barents Sea, in *Izuchenie glubinnogo stroeniya vostochnoi chasti Baltiiskogo shchita i prilegayushchikh akvatorii seismicheskimi metodami* (Seismic Studies of the Deep Structure of the Eastern Baltic Shield and Neighboring Marine Territories), Apatity: AN SSSR, 1986, pp. 91–100.

Pavlenkova, N.I., A three-dimensional model of the Baltic Shield crust from data of deep seismic studies, *Izv., Phys. Solid Earth*, 2006, vol. 42, no. 12, pp. 1007–1017.

Roslov, Yu.V., Sakoulina, T.S., and Pavlenkova, N.I., Deep seismic investigations in the Barents and Kara seas, *Tectonophysics*, 2009, vol. 472, pp. 301–308.

Sakulina, T.S., Telegin, A.N., and Tikhonova, I.M., Deep seismic studies on the geophysical Zapolyarnyi–Heisa reference profile, *Izv., Phys. Solid Earth*, 1999, vol. 35, no. 9, pp. 760–769.

Sakoulina, T.S., Telegin, A.N., Tichonova, I.M., Verba, M.L., Matveev, Y.I., Vinnik, A.A., Kopylova, A.V., and Dvornikov, L.G., The results of deep seismic investigations on geotraverse in the Barents Sea from Kola Peninsula to Franz Joseph Land, *Tectonophysics*, 2000, vol. 329, pp. 319–331.

Sakulina, T.S., Roslov, Yu.V., and Ivanova, N.M., Deep seismic investigations in the Barents and Kara seas, *Izv., Phys. Solid Earth*, 2003, vol. 39, no. 6, pp. 438–542.

Sakulina, T.S., Roslov, Yu.V., and Pavlenkova, G.A., Methods and results of processing of complex seismic investigations on the 2-AR profile (Barents–Kara shelf), *Izv., Phys. Solid Earth*, 2009, vol. 45, no. 3, pp. 231–238.

Sakulina, T.S., Pavlenkova, G.A, and Kashubin, S.N., Structure of the Earth's crust in the northern part of the Barents–Kara region along the 4-AR DSS profile, *Rus. Geol. Geophys.*, 2015, vol. 56, no. 11, pp. 1622–1633.

Tulina, Yu.V., The crustal structure along the DSS-76 profile in the version of sharply contrasting layered–block model, in *Izuchenie glubinnogo stroeniya vostochnoi chasti Baltiiskogo shchita i prilegayushchikh akvatorii seismicheskimi metodami* (Seismic Studies of the Deep Structure of the Eastern Baltic Shield and Neighboring Marine Territories), Apatity: AN SSSR, 1986, pp. 78–91.

Verba, M.L. and Matveev, Yu.I., Evolution of the Earth's crust of the Barents shelf based on the deep seismic studies, *Reg. Geol. Metallog.*, 2000, no. 12, pp. 175–185.

Verba, M.L., Ivanova, N.M., Katsev, V.A., Roslov, Yu.V., Sakulina, T.S., and Telegin, A.N., Results of seismic studies on the reference profiles AR-1 and AR-2 in the Barents and Kara seas, *Razved. Okhr. Nedr*, 2001, no. 10, pp. 3–7.

Verba, M.L., *Sravnitel'naya geodinamika Evraziiskogo basseina* (Comparative Geodynamics of Eurasian Basin), St. Petersburg: Nauka, 2008.

Zelt, C.A. and Ellis, R.M., Practical and efficient ray tracing in two-dimensional media for rapid traveltime and amplitude forward modeling, *Can. J. Explor. Geophys.*, 1988, vol. 24, no. 1, pp. 16–31.

Translated by M. Nazarenko